Cellulose
https://doi.org/10.1007/s10570-026-07264-0

ORIGINAL RESEARCH

Digital image correlation (DIC) analysis of regenerated cellulose (viscose) woven composites: orientation-dependent mechanical properties and poisson's ratio variations

Muhammad Sohaib Anas · Maximilian Pramreiter · Ulrich Müller · Bernhard Ungerer

Received: 6 November 2025 / Accepted: 8 October 2026
© The Author(s) 2026

Abstract This study investigates the anisotropic mechanical behavior of plain 1/1 woven regenerated cellulose composites, focusing on the influence of yarn orientation on tensile stiffness and strength, the composite toughness in the form of work of fracture and Poisson's ratio. The latter of which has not been investigated so far in the context of cellulose multifilament yarns. For this reason, a method using Digital Image Correlation (DIC) was established to provide a 3D high-resolution strain mapping. The results reveal a high sensitivity of the Poisson's ratio towards changes in yarn orientation making the weaving structure an essential design parameter in the engineering of bio-based lightweight composites. At 0 and 90°, the composites exhibit low Poisson's ratios (0.08 and 0.12), high stiffness (up to 7.1 GPa), and tensile strength (up to 170 MPa), but display brittle failure modes. Intermediate orientations, particularly 45°, demonstrate higher Poisson's ratios (~ 0.9), improved work of fracture values (up to 9000 J). Conversely, the 60° orientation shows the lowest mechanical properties, with stiffness and tensile strength dropping to 3.1 GPa and 50 MPa, respectively, due to critical misalignment effects. Seeking an optimum energy uptake for lightweight composites under tensile loads, orientations of 45° should be considered while intermediate orientation of 60° feature adverse strength to toughness relations. The findings contribute to the understanding of regenerated cellulose composites, which offer competitive mechanical properties, biodegradability, and sustainability, making them suitable for lightweight structural applications.

Keywords Anisotropic behavior · Deformation behavior · Mechanical characteristics · Poisson's ratio · Sustainable composites

M. S. Anas
Faculty of Mechanical Engineering and Design, Kaunas University of Technology, Kaunas, Lithuania

M. S. Anas · M. Pramreiter · B. Ungerer
Department of Natural Sciences and Sustainable Resources, Institute of Wood Technology and Renewable Materials, BOKU University, Konrad Lorenz-Strasse 24, A-3430 Tulln an Der Donau, Austria

M. Pramreiter
Department of Environmental Science, Policy and Management, Rausser College of Natural Resources, University of California Berkeley, Berkeley, CA, USA

U. Müller
Wood Vision Lab GmbH, Franz-Pichler-Straße 30, 8160 Weiz, Austria

B. Ungerer (✉)
Material Technology Innsbruck (MTI), University of Innsbruck, Technikerstraße 13, 6020 Innsbruck, Austria
e-mail: Bernhard.Ungerer@uibk.ac.at

Published online: 23 October 2026

Introduction

Composite materials play a critical role in modern engineering due to their unique combination of high strength, low weight, and customizable properties (Gay 2022a). These materials are composed of a matrix and reinforcement, which together provide enhanced performance compared to their individual components (Gay 2022b). Flexibility of these materials to develop custom design and properties has made them compulsory in industries where achieving an optimal balance of efficiency, durability, and performance is essential, considering for instance the aerospace or automotive sector (Bhong et al. 2023). By tailoring the selection of fiber and matrix, composites can be designed to deliver specific properties, such as high stiffness for structural applications or superior impact resistance for protective systems (Sun et al. 2018). Among composite materials, woven composites have received considerable attention in materials science due to their adjustable mechanical properties (Rajesh et al. 2018; Elfaleh et al. 2023). The inherent structural anisotropy and complex construction of woven fabrics, however, pose challenges in accurately characterizing their mechanical behavior, including properties like stiffness, tensile strength, and Poisson's ratio, which are crucial for predicting the performance under various loading conditions (Osada et al. 2003; Venkateshwaran et al. 2012).Traditional methods (strain gauge, extensometer or video extensometer) of measuring mechanical properties often fall short in providing accurate strain distribution across the composite surface because strain gauges provide localized measurements (1–2 mm area), extensometers offer averaged strain over a larger zone but remain spatially limited, video extensometers only capture average axial strain between gauge marks, which can overlook local variations. Electronic Speckle Pattern Interferometry (ESPI) offers nanometer-level sensitivity for very small displacements, but DIC is a better choice for composite testing due to its practicality and ability to reveal strain localization and damage evolution. where strain spreads unevenly because stiff fibers resist deformation, while the softer resin accommodates more strain, leading to heterogeneous strain fields and local concentrations around fibers and interfaces.

Digital Image Correlation (DIC) is a non-contact optical technique that measures 2D or 3D deformations by analyzing images captured from multiple cameras. By tracking the motion of a speckle pattern applied to the specimen's surface, DIC combines the perspectives from at least two cameras to triangulate the 3D displacement field. This stereo-vision approach allows for the reconstruction of full-field deformation, including in-plane and out-of-plane displacements, providing comprehensive strain and deformation measurements (Duchene et al. 2018) (Ziaja et al. 2024). For woven-based composites, DIC allows the visualization of inter-yarn interactions and localized deformations, contributing to a more comprehensive understanding of how these materials behave under various loading scenarios (Janeliukstis and Chen 2021). Through DIC analysis, it is possible to pinpoint areas of stress concentration, assess interlaminar failure modes, and observe the influence of fiber orientation on strain distribution (Bassir et al. 2024). DIC can help to reveal progressive microcracking along fiber boundaries in woven composites under cyclic loading and offers a real-time view of damage propagation helping to predict the lifespan of a composite element (Zhao et al. 2022). The non-destructive nature of DIC allows repeated testing on the same specimen and provides a continuous view of mechanical property changes over time (Naufal et al. 2024).

Accurate measurement of Poisson's ratio in woven composites remains challenging due to their inherent directional dependence (anisotropy) and complex microstructure. Unlike homogeneous materials, the interlacing fibers and resin-rich zones create non-uniform strain distributions, leading to variations in Poisson's ratio depending on loading direction and fiber orientation (Choi et al. 2023). Unlike isotropic materials, woven composites display variable strain responses depending on the fiber orientation and weave patterns. By tracking both longitudinal and transverse strains in real-time, DIC can provide a detailed strain map of woven composites and reveals how strain variations influenced by fiber arrangement and weave patterns (Islam et al. 2024). Poisson's ratio in woven composites is not uniform across the material but instead shows direction-specific behavior influenced by fiber/yarn orientation (Wei and Edwards 1998). DIC captures these variations effectively and offers precise measurements which would be difficult to achieve with traditional extensometers (Alderson, Alderson 2007). Strain concentrations

near crimped regions can significantly alter the effective Poisson's ratio, a phenomenon that traditional strain gauges often miss (Nazir et al. 2019). Through non-contact monitoring, DIC can track Poisson's ratio progress under cyclic loading (Nguyễn et al. 2023).

Regenerated cellulose composites behave differently from synthetic ones because the fibers are less stiff, more ductile, and bond better with epoxy (Pickering et al. 2016). This leads to unique strain and failure patterns in woven structures, where yarn orientation strongly affects the mechanical response. Despite the widespread application of woven fabric composites, a deeper understanding of their anisotropic mechanical behavior is still missing. How does yarn orientation influence the tensile properties, strain distribution, and Poisson's ratio of regenerated cellulose woven fabric composites? Critical aspects, such as the impact of yarn orientation on stiffness, Poisson's ratio or failure resistance remain underexplored in current research. This study examines the deformation behavior of plain 1/1 regenerated cellulose (viscose) woven fabrics composites. Regenerated cellulose filaments can offer unique advantages including biodegradability, reduced carbon footprint, and good interfacial adhesion with epoxy matrices while maintaining competitive mechanical properties, suitable for light weight structural applications. The investigation focuses on the deformation behavior of woven composites consisting of epoxy-impregnated, continuous regenerated cellulose filaments under tensile loading. Using Digital Image Correlation (DIC), mechanical properties, deformation behavior, and Poisson's ratio of plain 1/1 woven fabric composites were evaluated. Samples of regenerate cellulose plain 1/1 woven fabric composite were prepared and cut at an interval of 15° from 0° to 90° with respect to the warp yarn. By systematically analyzing the mechanical behavior across various orientations, this study contributes valuable insights for optimizing both the sustainability and performance of regenerated cellulose composites for structural applications.

Materials and Method

Material

In this study, high strength regenerated cellulose (viscose) in the form of plain 1/1 weave fabric was used as a reinforcement for the development of composite. This fabric was provided by Indorama Ventures Mobility Bohemia s.r.o. (Lovosice, Czech Republic). Instead of twisted filament yarns, straight filaments in the form of tapes were used Fig. 1. For the formation of this tape, viscose filaments are combined with polyurethane filaments (7.5% by weight), which act as a binder and form a stabilizing layer around the viscose filaments upon heating, a patent process, patent number WO 2024/223509 (Hehn et al. 2024). The polyurethane component (7.5 wt%) was not intended to replace the epoxy as the matrix phase. The linear density of

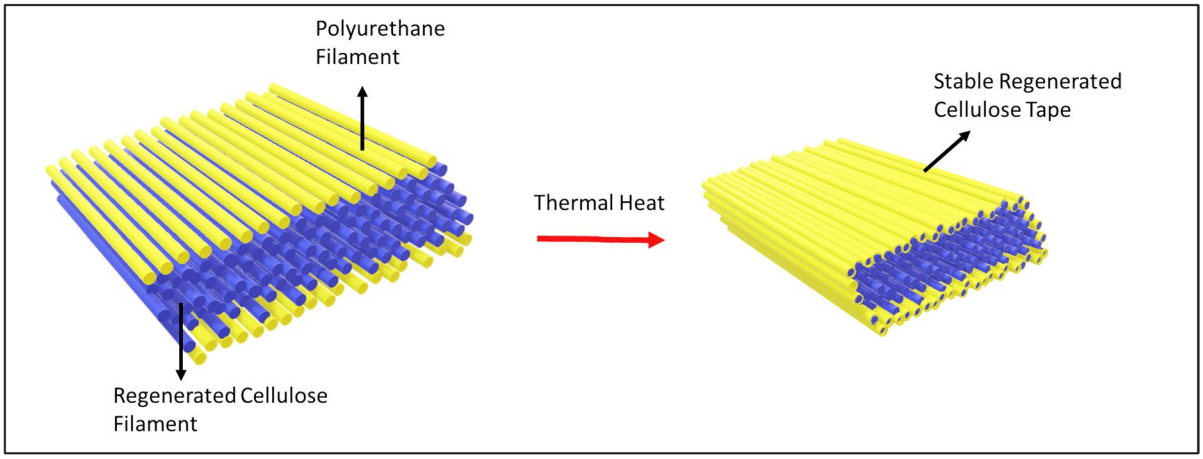


Fig. 1 Process of tape formation from regenerated cellulose filaments

the single viscose tape was 2440 dtex having 1320 filaments. The mechanical properties of all reinforcements are highlighted in Table 1. A two-component epoxy resin (Epoxidharz L + hardener GL 2) from R&G Faserverbundwerkstoffe GmbH, Germany with a mixed viscosity at 25 °C of 248 mPas was used as a matrix. In the final composite, epoxy remained the primary matrix, while the orientation-dependent deformation behavior and Poisson's ratio were mainly governed by the woven architecture and yarn alignment.

Table 1 Mechanical properties of regenerated cellulose's (viscose) fabric based on EN ISO 13934–1

Characteristics	Regenerated cellulose (viscose) plain (1/1)
Grams per square meter (GSM) (g/m^2)	217
Elastic modulus (GPa)	2.8
Tensile Strength (MPa)	112
Toughness at maximum load (Nmm)	3185
Toughness to failure (Nmm)	3833
Thickness (mm)	0.33

Sample preparation

The hand layup technique was used to prepare the composites. First, the epoxy resin was prepared as per the instructions given by the manufacturing industry with a ratio of 100:30 (resin:hardener), mixed properly, and then left for 10 min. After that, epoxy resin was poured on the fabric and spread evenly with the help of a roller. The composite was pressed under room temperature at 1.9 N/mm^2 pressure using a Hot Press (Langzauner LZT-160-SFB, Maschinenfabrik Langzauner GmbH, Lambrechten, Austria). The stamp size of the press was 180×300 mm^2. Samples were kept under pressure for at least 3 days until they were fully cured. Composite sheets were then left for one day in the climate room under standard conditions of temperature and relative humidity i.e., (20±2C and 65%±5%).Then, the composite sheet was cut at 7 different angles from 0° to 90° with an interval of 15° based on the orientation of the warp yarn as shown in Fig. 2. All test specimens were cut

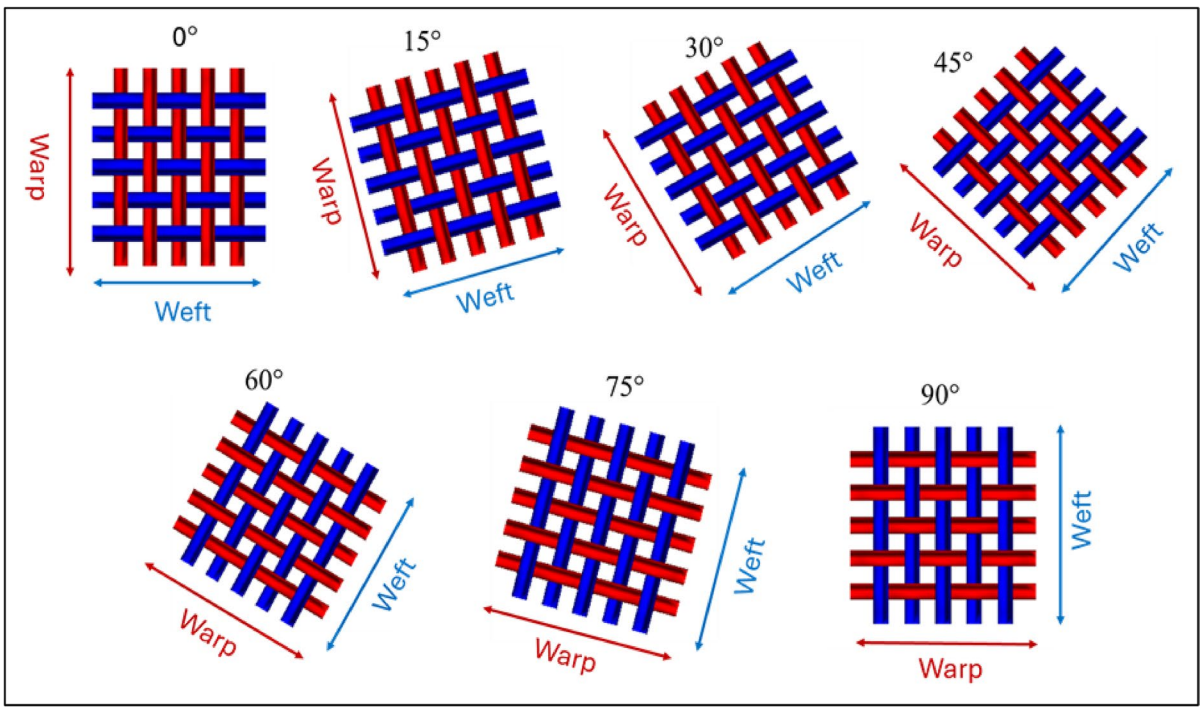


Fig. 2 Illustration of samples cut at different angles

from the same consolidated composite laminate produced during the hot-pressing process. Therefore, the specimen thickness, fiber-matrix ratio, and composite density remained identical for all orientations, and only the cutting angle relative to the warp yarn direction (0°–90°) was varied. For 0° and 90° orientations, the specimens contained 11 viscose tapes across the specimen width, ensuring consistent reinforcement distribution. For the other orientations (15°–75°), the specimen width was kept constant. The warp yarn direction of the woven fabric was used as the reference axis and prepared by marking the required angles relative to the warp direction using a precision protractor template, followed by cutting which maintained a comparable cross-sectional area for all samples during tensile testing. Before testing, a protective layer of beech veneers was applied at the ends of the cut samples using a single-component polyurethane to avoid sample failure in the clamping area. The design of the experiment includes seven different types of samples with at least 5 repetitions of each to account for material variability and to ensure statistical reliability. Each sample was assigned a code based on its angle with respect to the warp yarn (e.g., 0° for a fabric at 0-degree warp angle and 90° is for fabric at 90-degree warp angle).

Mechanical Characterization

The mechanical testing of the composites was done according to the ASTM D3039 with a universal testing machine (Z100; Zwick/Roell, Ulm, Germany), running the software testXpert III (Zwick/Roell,Ulm, Germany) and additionally equipped with an interface to directly transmit and synchronize the information about the forces detected by the DIC device Q-400 (Dantec Dynamics, Aalborg, Denmark) operated using Istra 4D software (version 4.9). Imaging was performed using a pair of synchronized Basler acA4112-30 um cameras, each equipped with a 1" Sony CMOS sensor providing a resolution of 4112×3008 pixels ($\approx$ 12.4 megapixels). The cameras were fitted with Schneider-Kreuznach Xenoplan 2.0/50 1220 HV lenses, which offer high optical precision and are optimized for industrial environments with vibration. These lenses provided minimal distortion and high contrast, enabling accurate subpixel correlation of speckle patterns. The distance from the cameras to the specimen surface (Standoff distance) was maintained at approximately 10–11 cm, with a baseline (distance between the two lenses) of 4–5 cm. The optical axes of the cameras were converged toward the specimen at a stereo angle of approximately 15–20°, optimized for accurate 3D reconstruction. The cameras were calibrated using a standard calibration screen (GL-06-BMB-9×9) through the software Istra4D 4.9.

The prepared samples were coated with a speckle pattern (a random, high-contrast pattern applied to a specimen's surface) using normal black spray paint to create a random pattern for the DIC system to track deformation during testing Fig. 3. Random speckle patterns generated using spray paint are a standard and cost-effective method in DIC experiments. This approach has been validated in numerous studies (Baran et al. 2017; Feng et al. 2022). The samples were then clamped into the tensile grips, ensuring a straight alignment to avoid skewed results. Two uniform LED panels were used to ensure homogenous illumination of the specimen surface. Before the test, a preload of 50 N was applied to remove slackness and ensure proper grip contact. Synchronized DIC system with the Zwick 100 machine record surface displacement at each time step as the load increased. The recording sequence speed was set to capture one image per second during the tests. For analyzing the images, the area of interest was marked for all samples, and evaluation settings (Facet size 29 pixels, grid spacing 17 pixels) were kept consistent. Facet size refers to the square area of pixels selected for tracking a pattern on the sample's surface while grid spacing is the distance between the centers of adjacent facets.

Working Principle of Digital Image Correlation (DIC)

Digital Image Correlation (DIC) works by capturing a series of images of a specimen surface as it undergoes deformation. The process begins by capturing a reference image, which displays the material in its original & undeformed state. As the test progresses subsequent images are compared to the referenced image and track changes on the surface. A random speckle pattern applied to the surface helps the system identify and follow specific areas, called subsets, throughout the deformation. A subset is a small square or rectangular region of pixels selected from the reference

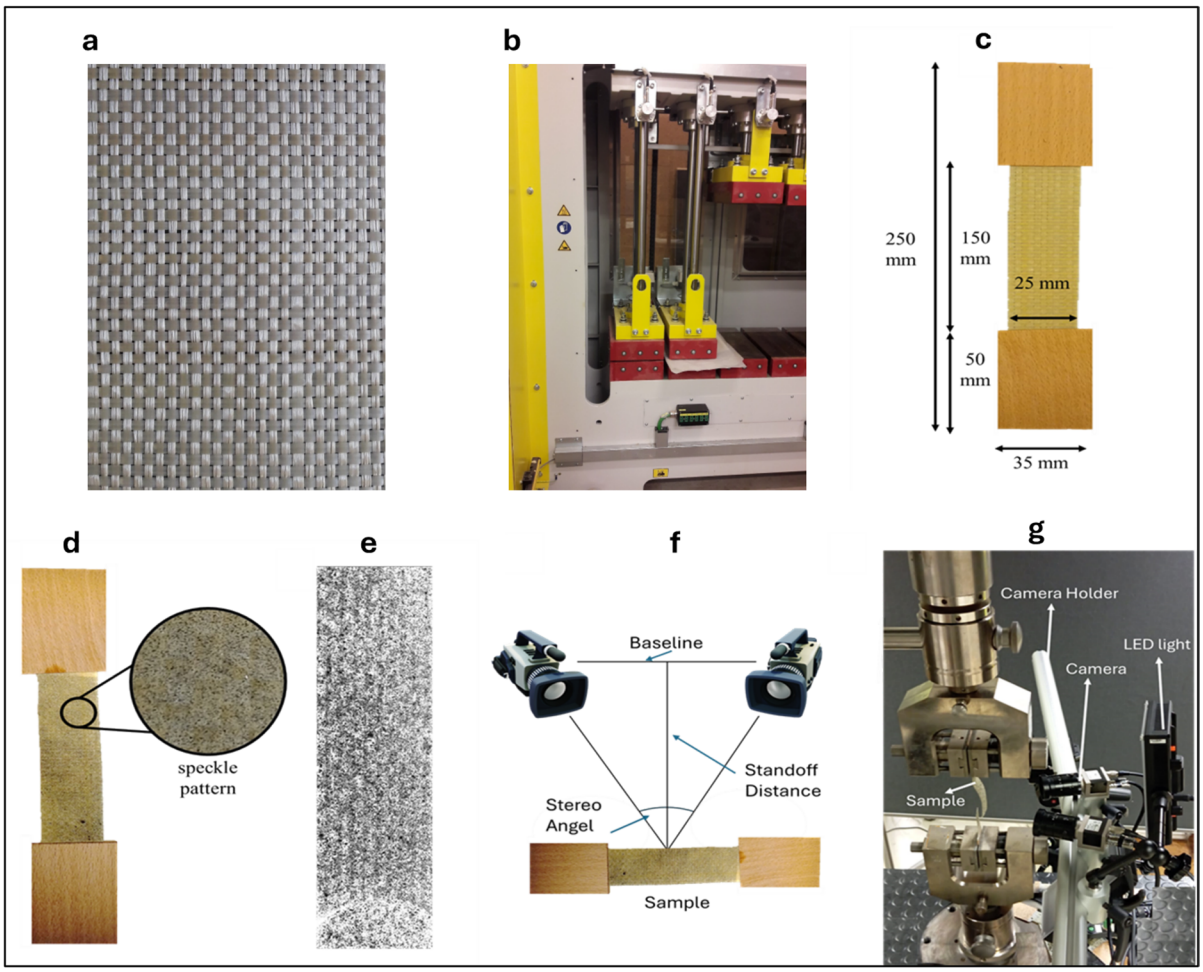


Fig. 3 Digital Image Correlation (DIC) setup for tensile testing of composite specimens **a** regenerated cellulose fabric, **b** composite sheet development, **c** prepared specimen for tensile test, **d** speckle pattern on sample surface, **e** reference image view from Istra 4.9 software, **f** schematic diagram of stereo camera setup, **g** actual experimental setup with cameras, light, and tensile machine

image. The software finds where this subset moved in the deformed image by matching pixel patterns. By correlating the subsets detected by cameras from different angles, the system creates a 3D model of the surface. The movement and deformation of each subset are determined by tracking changes in the brightness of pixels within the images. By comparing the changes between the reference and deformed states, the software (Istra4D 4.9) calculates displacement and strain on the surface and provides precise data about how the material responds to the tensile loads applied. Consistent facet size, grid spacing, lighting conditions, and camera alignment were maintained for all tests to ensure reliable strain evaluation.

To capture localized deformation, engineering principal strain maps were generated. Principal strain represents the maximum localized stretching or compression within the material, and in composites especially under off-axis loading its distribution and orientation provide valuable insight into the underlying deformation mechanisms. These strain maps were used to identify regions of concentrated stress, enabling the detection of potential crack initiation sites and failure paths.

Calculation of Poisson's Ratio

In the Istra 4.9 digital image correlation (DIC) software, the surface of a test specimen divided into a grid of sub-regions (facets) to facilitate high-resolution deformation analysis under uniaxial tensile loading. Software tracks the displacement of each facet by correlating speckle patterns captured via high-resolution imaging. From these displacement fields, Istra 4.9 computes the longitudinal strain along the loading axis and the transverse strain perpendicular to it. Poisson's ratio for each facet is calculated as the negative ratio of transverse to longitudinal strain as shown in Fig. 4 where mstrain stands for microstrain, 1 mstrain (or $\mu\varepsilon$) $= 1\times10^{-6} = 0.000001$. This process yields a spatially resolved map of Poisson's ratio, enabling visualization of its heterogeneity across the specimen surface. Poisson's ratio was determined using averaged strain values from the central region of interest, while edge regions near the grips were excluded to avoid boundary effects and noise in the DIC measurements. Software also has the capability to compute an average Poisson's ratio over a user defined region of interest, while retaining the detailed spatial distribution for localized analysis. This function supports comprehensive material characterization and detailed investigation of microstructural variations.

Results and discussion

Mechanical properties

There are high differences in variability of properties (Fig. 5), since the specimens were cut at different orientations, there is always a probability that same angel samples cannot be cut at exactly same fiber volume fraction. Due to this microstructural variability within the woven composites play it part by changing yarn crimp, waviness, and resin-rich pockets. The mechanical properties, energy absorption and deformation pattern of plain-woven fabric composites change significantly depending on the yarn orientation in tensile direction, which influence how load is distributed across the material as shown in Fig. 6. At 0° orientation, the warp yarns are aligned with the loading direction and therefore act as the dominant load-bearing component. This results in the highest average stiffness (7.1 GPa) and tensile strength (170 MPa). At this angle composites fail in an abrupt and brittle way, because the warp yarns dominate the load-bearing capacity, and the matrix has little involvement as compiled in the fracture patterns in Fig. 7**.** In return, the work of fracture is relatively low (5000 J) because of minimal deformation and crack resistance (de Paiva et al. 2006). As the yarn orientation shifts to 15° and 30°, mechanical response becomes more complex. The direct alignment of warp yarns with the load decreases, and the role of off-axis (weft) yarns and matrix deformation increases. 84% warp and 16% weft by mass in 15°, and 66% warp and 34% weft in 30°, (these % figures

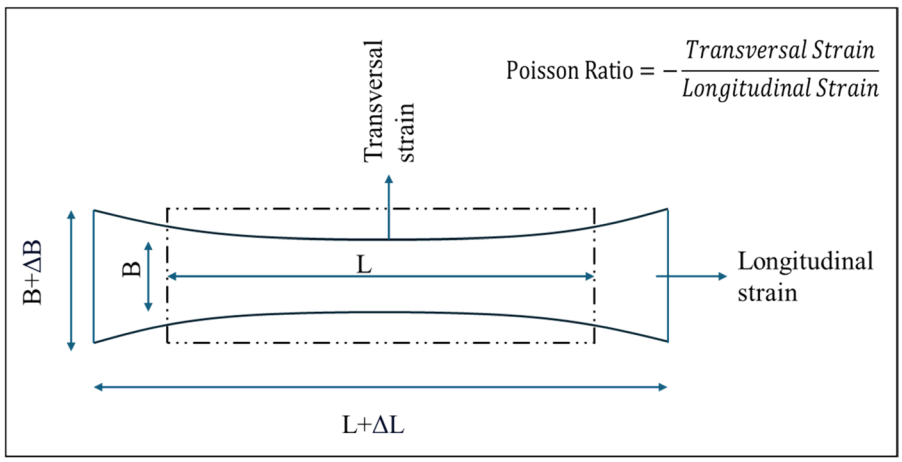


Fig. 4 Calculation of Poisson's ratio

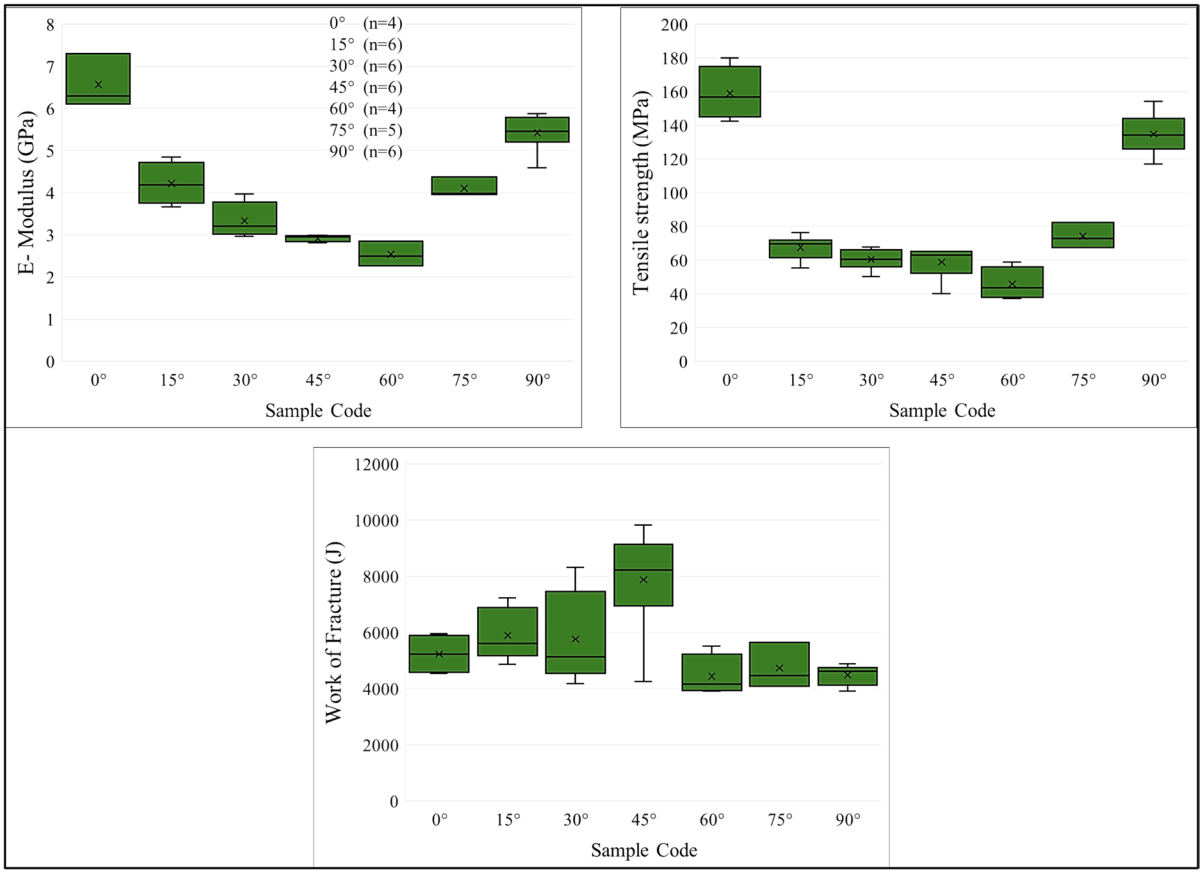


Fig. 5 Mechanical properties of regenerated cellulose composites samples

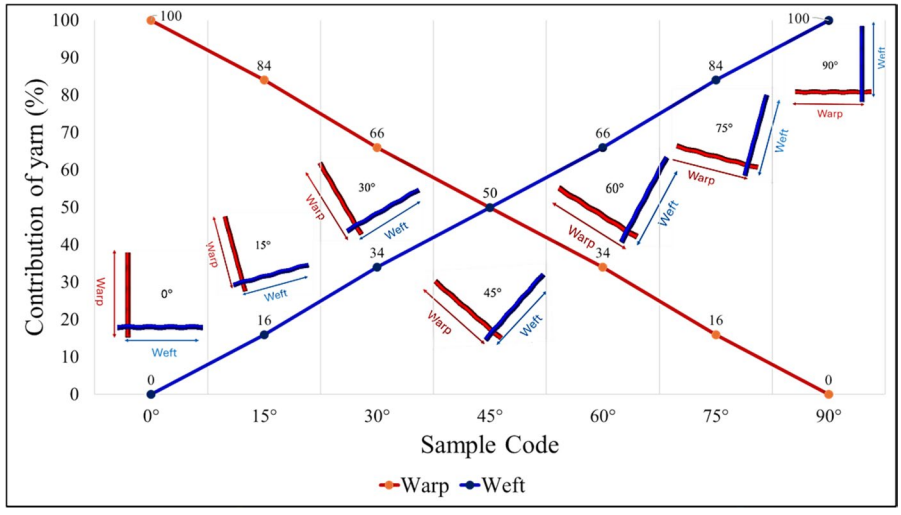


Fig. 6 Estimated contribution of warp and weft yarn on mechnical properties of plain woven fabric composites

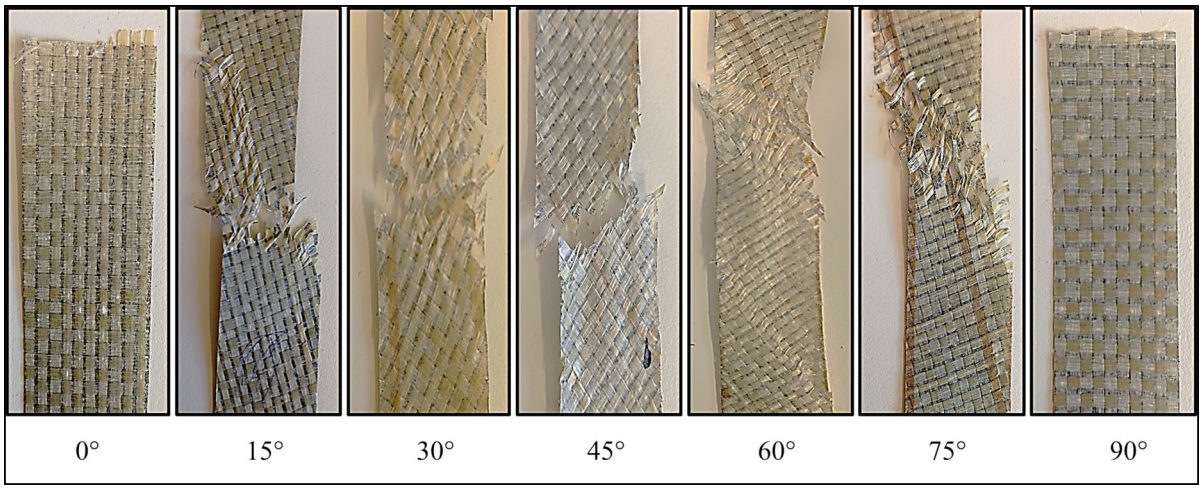


Fig. 7 Tested samples showing deformation behavior of samples with respect to the angle

represent estimated material proportions, based on the geometric orientation of the yarn systems relative to the loading direction, not a direct distribution of mechanical contribution) and this results in a reduced stiffness and strength as warp yarns are no longer fully aligned with the load. At this stage the mechanical behavior of regenerated cellulose plain 1/1 woven composites is strongly influenced by yarn orientation and composite's ability to absorb energy improved as the work of fracture increases to 6500 J and 7500 J for 15° & 30° respectively, because the matrix undergoes progressive cracking, allowing more energy to dissipate through the composite during failure (He et al. 2020). The deformation behavior of samples becomes more noticeable, with wearing out of yarns and some splitting. At 45°, warp and weft yarns share the load equally (50% each), creating a balance of strength, deformation, and energy absorption. Work of fracture was highest at this angle (9000 J). This results in yarn pull-out, and widespread deformation before failure, making the material more tough (Pan et al. 2009). While stiffness (3.6 GPa) and tensile strength (60 MPa) are lower compared to the samples at 15° and 30°.

At 60° yarn orientation, the loading direction diverges from the warp alignment, and more load being transferred to the weft yarns. Unlike the warp yarns, which are typically straighter and stiffer, the weft yarns have higher crimp due to the weaving process inducing inherently lower stiffness. As a result, although the weft yarns begin to contribute more to load transfer at this angle, their crimped structure leads to more deformation and a pronounced shear response. Although it might expect 45° to yield the lowest properties but combined effect of misalignment of warp yarns, activation of crimped weft yarns, and increased shear lead to lower overall stiffness in the 60° sample compared to all other orientations. Stiffness and strength drop to their lowest levels (3.1 GPa and 50 MPa), and the work of fracture is also low (4500 J) (Munro et al. 1997; Lomov et al. 2000). At 75° weft yarns dominate further, contributing 84%, while the warp yarns contribute just 16%. The better alignment of weft yarns with the load direction improves stiffness (5.2 GPa) and tensile strength (90 MPa), and the work of fracture rises to 5000 J. Deformation becomes more uniform, with less damage to samples compared to 60°. Finally at 90°, At 90° orientation, the weft yarns become the dominant load-bearing component, while the matrix and warp yarns contribute indirectly through stress transfer and structural constraint. The stiffness (6.8 GPa) and tensile strength (150 MPa) are slightly lower than at 0° because the weft yarns have more crimps than the warp yarns, reducing their effectiveness (Ungerer et al. 2022). The work of fracture drops again to 4500 J, with failure being clean and dominated by the yarns. Plain-woven composites' mechanical properties depend strongly on yarn orientation relative to load direction. Aligned yarns provide maximum stiffness and strength but

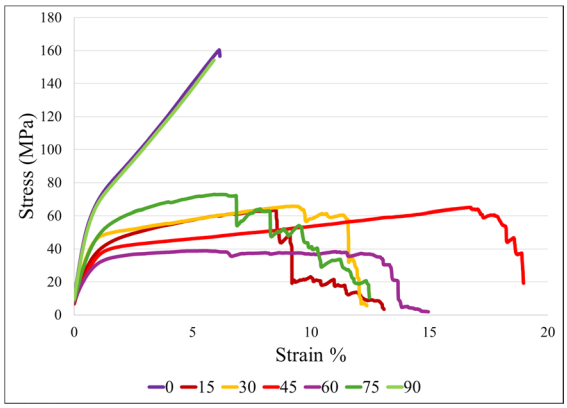


Fig. 8 Stress–strain curves of regenerated composites cut at different angles

fail brittlely. Off-axis orientations increase matrix involvement, improving energy absorption through cracking and yarn-matrix interactions. Balanced warp-weft loading enhances toughness, but extreme misalignment weakens performance when neither yarn system effectively engages. However, at certain orientations, like in case of 60° both warp and weft yarns were not aligned effectively, leading to reduced mechanical properties and early failure.

Figure 8 shows the stress–strain curves of representative specimen. These curves represent the best-performing samples (highest modulus) from each replicate tested in terms of mechanical properties. Since a total of 35 specimens were tested, plotting all curves would reduce figure readability. Therefore, the statistical variability of the mechanical properties is already presented separately using box plots in Fig. 5. The observed variation in stress–strain behavior with increasing orientation angle is related to the transition from fiber-dominated loading to shear-dominated deformation in the woven structure. At 0° and 90°, the composite is strongest and stiffest because the load aligns perfectly with either warp or weft yarns, but it is brittle with limited energy absorption. At intermediate angles, especially 45°, the balance between yarn and matrix contributions allows for better toughness and energy absorption, making the composite more resistant to damage. Poor alignment at 60° results in the weakest performance, showing that yarn orientation must be carefully tailored for specific applications to achieve the desired balance between strength, stiffness, and toughness. As the angle increases further toward 75°–90°, the weft yarns become more aligned with the loading direction, which explains the recovery in mechanical properties.

Poisson's ratio

Poisson's ratio behavior of the regenerated cellulose composites exhibits remarkable orientation-dependent characteristics, demonstrating the samples pronounced anisotropic nature., as shown in Fig. 9. At 0° orientation the yarns are fully aligned with the loading direction, composite shows a mean longitudinal strain of 70.82 mstrain, accompanied by a minimal transverse contraction of −5.77 mstrain, resulting in a notably low mean Poisson's ratio of 0.08. Composites reinforced with highly aligned yarns; the tensile load is predominantly carried by the yarns due to superior axial stiffness. This efficient load-bearing mechanism significantly limits the overall deformation of the composite under tensile stress. Matrix contributes minimally to load resistance; the system exhibits restricted plastic deformation and low energy absorption. Once the tensile capacity of the yarns is exceeded, the composite fails abruptly, displaying a brittle fracture with little prior strain. Poisson's ratio in such systems tends to be low and positive, as the yarns stiffness constrains lateral contraction during axial loading. Results in a (positive) Poisson effect, a characteristic of anisotropic fiber-reinforced composites (Fang et al. 2022). Mean Poisson's ratio (Fig. 10) increases to 0.63 at 15° reflecting the effect of yarn misalignment. The longitudinal strain is similar to the 0°, with a mean value of 69.41 mstrain, but the transversal strain becomes more pronounced around −43.75 mstrain. The effect becomes more pronounced at 30°, where the Poisson's ratio rises to 0.83. Here, the longitudinal strain also increases slightly to 74.57 mstrain, while the transverse strain reaches−63.01 mstrain, suggesting that the shear deformation mechanisms become more dominant as the yarn orientation diverges further from the loading axis.

At a yarn orientation of 45°, which corresponds to the principal direction of maximum in-plane shear stress in composite laminates, Poisson's ratio reaches a peak value of 0.90. This orientation also results in the highest measured strain values 148.16 mstrain in the longitudinal direction and −135.14 mstrain in the transverse direction. The 45° alignment represents

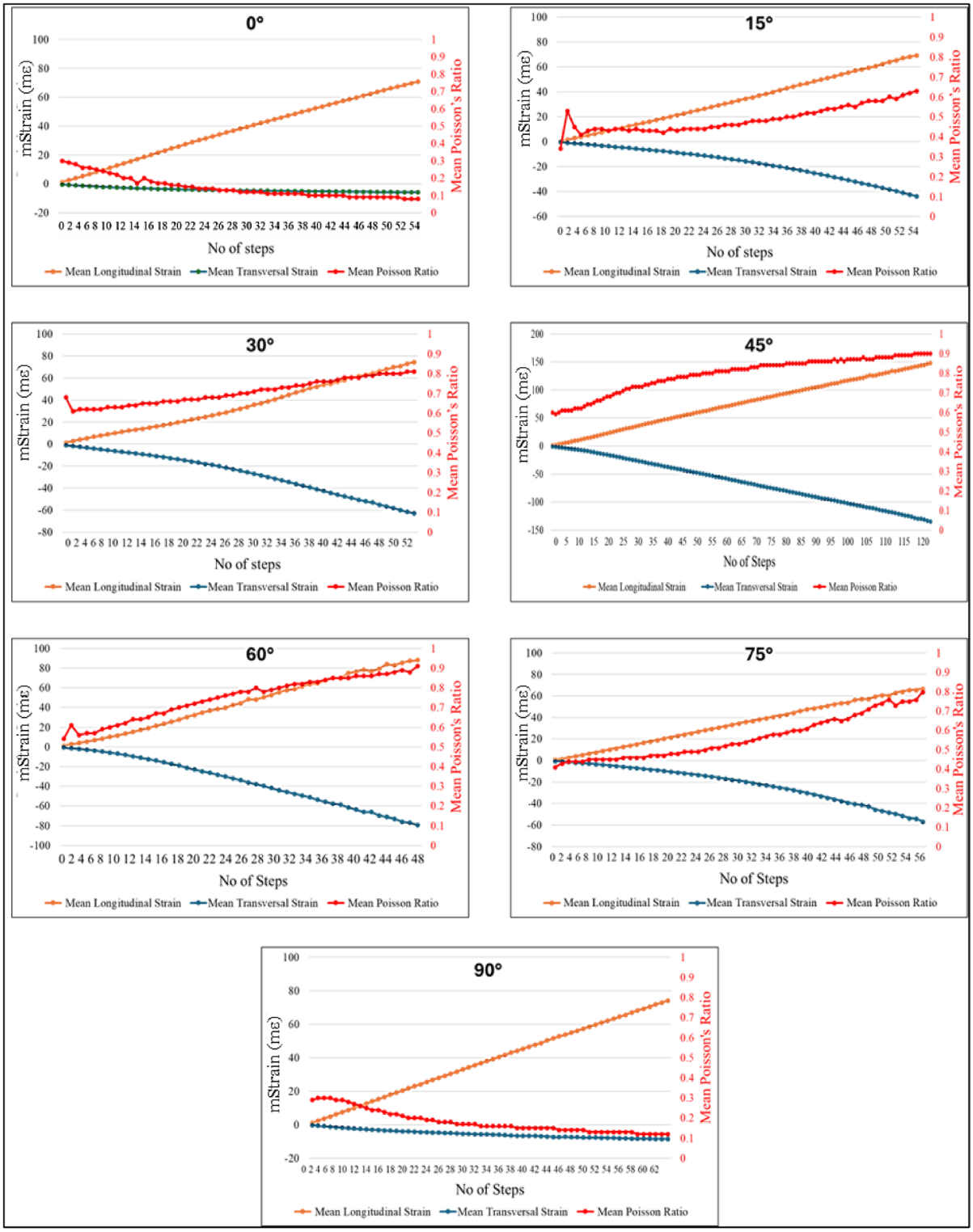


Fig. 9 Poisson's ratio of plain weave fabric regenerated cellulose composites

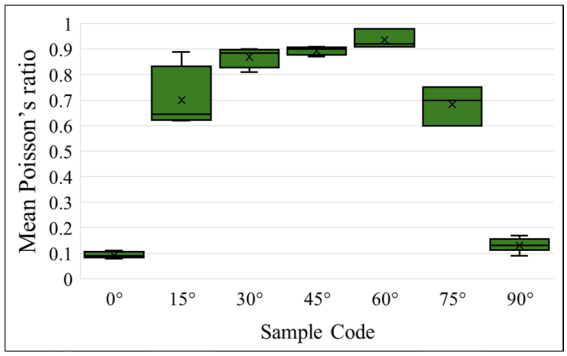


Fig.10 Poisson's ratio distribution of samples

the condition under which axial stresses are most effectively transformed into shear stresses within the composite. The deformation response is primarily governed by matrix shear and yarn angle, as axial stiffness is no longer the dominant factor. This shear-dominated state leads to transverse contraction, explaining the elevated Poisson's ratio and strain levels (Mahfuz et al. 2004). Orientations at 60° and 75° maintain relatively high Poisson's ratios of 0.93 and 0.75, respectively, reflecting the continued dominance of shear and transverse deformation modes. At 90° orientation, again yarns are fully perpendicular to the load, the composite again shows a low Poisson's ratio of 0.12, with longitudinal strain of 74.13 mstrain and transverse strain of − 8.56 mstrain.

Compared to traditional composites like glass & carbon fiber, the plain 1/1 viscose/epoxy samples show comparative Poisson's ratios at 0° orientation (0.08) and 90° orientation (0.13), indicating good axial stiffness and minimal lateral deformation due to aligned viscose tapes. Carbon and glass fiber composites typically exhibit Poisson's ratios in the range of 0.10–0.40, at 0° (Craig and Summerscales 1988; Shan et al. 2022). Hemp-based natural composites, depending on fiber quality and orientation, usually present values around 0.30–0.40 (Yan et al. 2014). The much broader range observed in viscose/epoxy (from 0.08 to 0.91) highlights its pronounced anisotropic behavior under tensile loading, governed by yarn alignment mechanisms (Craig and Summerscales 1988). Orientation-dependent Poisson's ratio values can be crucial for accurately capturing the anisotropic deformation of composites. It can provide essential material inputs for finite element modeling (FEM) and laminate theory simulations, enabling precise prediction of stress, strain, and failure in fiber-reinforced laminates at varying fiber directions.

Strain distribution and failure mechanism

Figure 11 shows the Engineering principal strain distribution in composite samples of plain 1/1 weave viscose epoxy composite at different orientations with respect to warp yarns (0, 30°, 45°, 60°, 75°, and 90°) during tensile testing. The scale on the side of each image shows the values of the strain. The color coding indicates the magnitude of strain, with warmer colors (yellow and red) corresponding to higher strains, and cooler colors (blue and purple) indicating lower strains. The plain 1/1 weave pattern is characterized by the interlacing of yarns in a criss cross manner. At different angles of warp yarn, the interaction between the yarn orientation and the applied stress will vary, leading to different strain localized distributions. Strain localization is the concentration of deformation in specific regions of a composite under load, often occurring near matrix-rich areas or fiber interfaces. It signals the onset of damage such as matrix cracking or fiber breakage. In composites, this behavior is critical for identifying failure zones and is commonly observed as strain hotspots in DIC analysis.

At 0° yarn orientation (warp-aligned), these warp yarns bear the load, resulting in efficient load transfer and minimal overall deformation. The weft yarns, oriented perpendicular to the loading direction, contribute negligible to the mechanical force and remain unstressed. Shear deformation is minimal in this configuration, as the load is carried directly through the straight warp yarns without significant distortion. The strain distribution is primarily concentrated along the warp direction, reflecting the engagement of these yarns in resisting the applied stress. Strain levels are relatively low (0.1% to 2%) and uniformly distributed, with only minor localized strain variations observed near the central region of the specimen. This indicates that the composite maintains structural integrity and resists deformation effectively under axial loading. The failure mode at this orientation was tensile rupture of the warp yarns once their load-bearing capacity was exceeded (Patel and Peralta 2017). At 15°, the strain distribution is uneven, ranging from 0.5% to 2.5%. Load is still mainly carried by the warp yarns, because the warp yarns are still aligned with

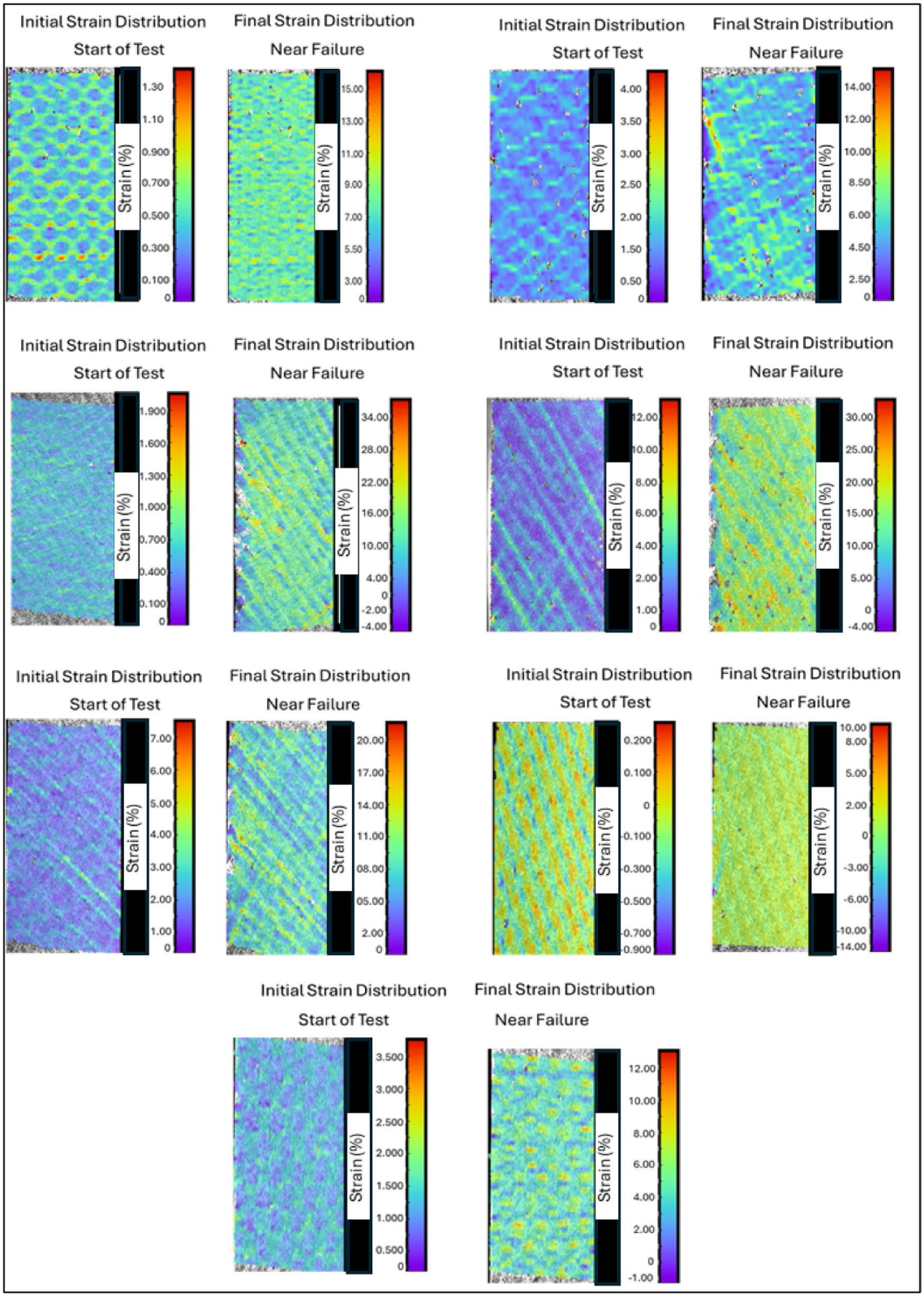
the load direction. Shear forces start to develop due to the angle between yarns and the load, leading to shearing deformation at yarn intersections. Failure is more ductile compared to 0°. As failure approaches, strain increases to 14%, weft yarns start to experience stress, though not as much as the warp yarns, and this results in an increased strain at the yarn intersections. Shear failure occurs at yarn intersections. Samples cut at 30° weave (moderate angle) load is shared more evenly between the warp and weft yarns than 15° samples. Material is subjected to higher shear forces, which leads to more distributed deformation. Yarns are no longer aligned with the applied load. Weft yarns are now engaging more in load transfer, and there is an increase in shear deformation in the weft direction. Strain distribution becomes more complex, and localized strain areas appear. The interface between yarns failed due to the shearing forces. Fiber-matrix debonding also occurs as the material is subjected to both tensile and shear stresses.

At 45°, the load is not aligned with the yarns in either direction. Strain ranges from 1 to 7% at the beginning, the load is more evenly shared between the warp and weft yarns. Material's stiffness significantly decreases, and the deformation becomes non-uniform. Material is much more flexible at this angle and experiences greater strain. As the test progresses, strain increases to 30%, with localized high-strain regions showing where cracks begin. The highest strain remains diagonal, aligned with the yarn direction, suggesting significant shear deformation within the matrix (Ge and Hu 2015). At 60°, the strain initially ranges from 2.5% to 6%, at this angle, the strain distribution is somewhat similar to the 30° and the matrix plays a larger role in transferring stresses due to the misalignment of both yarn systems with the applied load. As the test continues, strain increases up to 20%. The strain is relatively low, but more localized areas show higher strain. Neither is the yarn system well-aligned with the load, causing early strain localization and failure.

At 75°, strain is initially uniform, ranging from 0% to 0.5%, with the load being transferred mostly through the weft yarns, which are more aligned with the load direction. As the test proceeds, strain increases to 8% with strain concentrating along the weft yarn paths. The composite shows better energy absorption compared to the 60°. At 90°, strain starts at values between 0% and 1.2%, with the load mainly carried by the weft yarns, which are perfectly aligned with the applied load. This results in efficient load transfer, with little involvement from the matrix in the early stages. As the yarns reach their tensile strength, strain becomes localized, particularly along the weft yarns. The failure at 90° is brittle, dominated by yarn rupture(Holmes et al. 2020).

The mechanical behavior of regenerated cellulose plain 1/1 woven composites is strongly influenced by yarn orientation (Sohaib Anas et al. 2025), as demonstrated by the varying stiffness, strength, and failure modes across different angles. The highest stiffness and tensile strength at 0° and 90° align with previous studies on aligned fiber composites, where load transfer is most efficient along the principal fiber direction. However, the reduced performance at intermediate angles (15°–75°) reflects the increasing role of matrix, shear and yarn crimp. The observed peak in energy absorption at 45° can be attributed to the balanced contribution of warp and weft yarns, promoting progressive damage through matrix cracking and yarn pull-out rather than sudden yarn rupture. This behavior is like that seen in glass and carbon woven composites, where off-axis loading enhances toughness by activating multiple failure mechanisms (Karahan and Karahan 2013; Zhou et al. 2021; Wang et al. 2024). But exceptionally low performance at 60° suggests a critical misalignment threshold where neither yarn system effectively resists the applied load, leading to premature failure, a phenomenon less pronounced in synthetic fiber composites due to their higher inherent stiffness. Similar orientation-dependent responses have also been reported in conventional woven glass and carbon fiber composites under off-axis loading, where stiffness decreases at intermediate angles while energy absorption increases due to shear-dominated deformation mechanisms (Lomov et al. 2009). But compared with synthetic fiber systems, regenerated cellulose composites tend to exhibit greater deformation and matrix participation because of the lower stiffness and higher ductility of the cellulose filaments, which enhances toughness.

Poisson's ratio variations further underscore the anisotropic nature of these composites. The near-zero values at 0° and 90° are typical of highly aligned yarn systems, where lateral contraction is constrained by fiber rigidity. In contrast, the elevated Poisson's ratios at 45°–60° indicate significant shear-induced deformation. The strain distribution patterns, captured via DIC,


Initial Strain Distribution
Start of Test
Final Strain Distribution
Near Failure
Strain (%)
1.30
1.10
0.900
0.700
0.500
0.300
0.100
0
15.00
13.00
11.00
9.00
7.00
5.50
3.00
0
Initial Strain Distribution
Start of Test
Final Strain Distribution
Near Failure
Strain (%)
4.00
3.50
3.00
2.50
2.00
1.50
0.50
0
14.00
12.00
10.00
8.50
6.00
4.50
2.50
0
Initial Strain Distribution
Start of Test
Final Strain Distribution
Near Failure
Strain (%)
1.900
1.600
1.300
1.000
0.700
0.400
0.100
0
34.00
28.00
22.00
16.00
10.00
4.00
0
-2.00
-4.00
Initial Strain Distribution
Start of Test
Final Strain Distribution
Near Failure
Strain (%)
12.00
10.00
8.00
6.00
4.00
2.00
1.00
0
30.00
25.00
20.00
15.00
10.00
5.00
0
-4.00
Initial Strain Distribution
Start of Test
Final Strain Distribution
Near Failure
Strain (%)
7.00
6.00
5.00
4.00
3.00
2.00
1.00
0
20.00
17.00
14.00
11.00
08.00
05.00
2.00
0
Initial Strain Distribution
Start of Test
Final Strain Distribution
Near Failure
Strain (%)
0.200
0.100
0
-0.100
-0.300
-0.500
-0.700
-0.900
10.00
8.00
5.00
2.00
0
-3.00
-6.00
-10.00
-14.00
Initial Strain Distribution
Start of Test
Final Strain Distribution
Near Failure
Strain (%)
3.500
3.000
2.500
2.000
1.500
1.000
0.500
0
12.00
10.00
8.00
6.00
4.00
2.00
0
-1.00

◂**Fig. 11** Principal strain (%) distribution obtained from Digital Image Correlation (DIC) for specimens 0°, 15°, 30°, 45°, 60°, 75°, and 90° and show the strain fields at the initial deformation stage and at the final stage immediately before failure, corresponding to an applied engineering strain of 1%

reveal localized strain concentrations at yarn intersections in off-axis samples, confirming that stress redistribution occurs through matrix shear rather than direct yarn loading.

Conclusion

This study critically examines the anisotropic behavior of plain 1/1 woven regenerated cellulose composites, with a particular emphasis on mechanical properties, Poisson's ratio and deformation across different yarn orientations ranging from 0° to 90°. The application of Digital Image Correlation (DIC) provides high-resolution strain mapping and reveals that Poisson's ratio significantly differs with yarn orientation. Notably, at 0° and 90°, the composites exhibited low Poisson's ratios of approximately 0.08 and 0.12 respectively, highlighting the dominance of aligned warp and weft yarns in resisting lateral deformation. These orientations also demonstrated the highest stiffness (up to 7.1 GPa) and tensile strength (up to 170 MPa), but with limited energy absorption and brittle failure modes. On the other hand, intermediate yarn angles particularly 45° and 60° showed higher Poisson's ratios (~ 0.9 and ~ 0.91), these orientations gain improved energy absorption and toughness, and work of fracture values (up to 9000 J at 45°). At 60° orientation the composites exhibited the lowest mechanical properties, with stiffness and tensile strength dropping to 3.1 GPa and 50 MPa, respectively. Critical misalignment effect at 60°, where neither yarn system contributes effectively to load transfer. This distinct failure threshold has not been emphasized in prior literature and provides a design warning for applications relying on off-axis load paths. In contrast, the identification of 45° as the optimum orientation for energy absorption highlights opportunities to tailor fabric orientation for toughness and progressive damage tolerance.

Regenerated cellulose composites show competitive stiffness and their biodegradability and sustainable production make them viable for lightweight structural applications where moderate strength and environmental impact are prioritized. Future research can explore hybrid reinforcements, optimized weave architectures, and advanced resin systems to enhance mechanical performance while retaining sustainability benefits.

Acknowledgements This study was conducted as part of the Austrian Biorefinery Center Tulln (ABCT-II) research project. The support of the ABCT-II partner Indorama Ventures Schoeller Wool Austria GmbH in terms of the material supply is gratefully acknowledged and the authors would also like to thank Johannes Steindl and Walter Schalko from the ABCT-II project partner F.List GmbH for their valuable support

Author contribution Muhammad Sohaib Anas: Experimental Methods, Investigation, Data Analysis, Writing original draft. Maximilian Pramreiter: Review and editing, Data Analysis. Ulrich Müller: Conceptualization, Data Analysis, Project administration, Validation, Supervision. Bernhard Ungerer: Conceptualization, Data Analysis, Validation, Supervision, Review and editing

Funding Open access funding provided by University of Innsbruck and Medical University of Innsbruck. This study was funded by the province of Lower Austria (FTI-calls), University of Natural Resources and Life Sciences Vienna (BOKU), F.List GmbH and Indorama Ventures Schoeller Wool Austria GmbH. Open access funding was provided by University of Innsbruck.

Data availability The data supporting this study can be provided on request

Declarations

Conflict of interest The authors declare no conflict of interests

Ethical approval Not applicable, as the study does not involve human participants, animals, or any ethical approval requirements

Open Access This article is licensed under a Creative Commons Attribution 4.0 International License, which permits use, sharing, adaptation, distribution and reproduction in any medium or format, as long as you give appropriate credit to the original author(s) and the source, provide a link to the Creative Commons licence, and indicate if changes were made. The images or other third party material in this article are included in the article's Creative Commons licence, unless indicated otherwise in a credit line to the material. If material is not included in the article's Creative Commons licence and your intended use is not permitted by statutory regulation or exceeds the permitted use, you will need to obtain permission directly from the copyright holder. To view a copy of this licence, visit http://creativecommons.org/licenses/by/4.0/.

References

Alderson, Alderson (2007) Auxetic materials. J Aerosp Eng 221:565–575

Anas MS, Ungerer B, Al-Musawi H et al (2025) Regenerated cellulose as a sustainable alternative to glass fiber composites: effects of fabric structure and applied pressure during curing. Cellulose 32(6):4039–4056. https://doi.org/10.1007/S10570-025-06498-8

Baran I, Cinar K, Ersoy N et al (2017) A review on the mechanical modeling of composite manufacturing processes. Arch Comput Methods Eng 24:365–395. https://doi.org/10.1007/S11831-016-9167-2

Bassir D, Guessasma S, Zheng Y et al (2024) Composite characterization using digital image correlation (DIC) approach for stress-strain prediction. AIP Conf Proc. https://doi.org/10.1063/5.0213202/3297086

Bhong M, Khan TKH, Devade K et al (2023) Review of composite materials and applications. Mater Today Proc. https://doi.org/10.1016/J.MATPR.2023.10.026

Choi JY, Yanamandra K, Shetty A, Gupta N (2023) Measurement of viscoelastic constants and Poisson's ratio of carbon fiber reinforced composites using in-situ imaging. J Reinf Plast Compos 42:638–647. https://doi.org/10.1177/07316844221136843/ASSET/IMAGES/LARGE/10.1177_07316844221136843-FIG11.JPEG

Craig PD, Summerscales J (1988) Poisson's ratios in glass fibre reinforced plastics. Compos Struct 9:173–188. https://doi.org/10.1016/0263-8223(88)90013-X

de Paiva JMF, Mayer S, Rezende MC (2006) Comparison of tensile strength of different carbon fabric reinforced epoxy composites. Mater Res 9:83–89. https://doi.org/10.1590/S1516-14392006000100016

Duchene P, Chaki S, Ayadi A, Krawczak P (2018) A review of non-destructive techniques used for mechanical damage assessment in polymer composites. J Mater Sci 53:7915–7938. https://doi.org/10.1007/S10853-018-2045-6

Elfaleh I, Abbassi F, Habibi M et al (2023) A comprehensive review of natural fibers and their composites: an eco-friendly alternative to conventional materials. Results Eng 19:101271. https://doi.org/10.1016/J.RINENG.2023.101271

Fang S, Zheng X, Guo B et al (2022) Experimental investigation of double-sided strain of composites in tensile testing using multicamera DIC. Mater Eval 80:42–51. https://doi.org/10.32548/2022.ME-04283

Feng W, He P, Pavlovic M (2022) Combined DIC and FEA method for analysing debonding crack propagation in fatigue experiments on wrapped composite joints. Compos Struct 297:115977. https://doi.org/10.1016/J.COMPSTRUCT.2022.115977

Gay D (2022a) Composite Materials: Interest and Physical Properties. Composite Materials. https://doi.org/10.1201/9781003195788-2/COMPOSITE-MATERIALS-INTEREST-PHYSICAL-PROPERTIES-DANIEL-GAY

Gay D (2022b). Composite Materials : Design and Applications. https://doi.org/10.1201/9781003195788

Ge Z, Hu H (2015) A theoretical analysis of deformation behavior of an innovative 3D auxetic textile structure. J Text Inst 106:101–109. https://doi.org/10.1080/00405000.2014.906099

He W, Wang C, Wang S et al (2020) Characterizing and predicting the tensile mechanical behavior and failure mechanisms of notched FMLs—Combined with DIC and numerical techniques. Compos Struct. https://doi.org/10.1016/j.compstruct.2020.112893

Hehn D, Matyja A, Lindner M (2024) Cellulose Tape Yarn. World Intellectual Property Organization -WIPO. WO 2024/223509 A1. https://worldwide.espacenet.com/publicationDetails/biblio?FT=D&date=20241031&DB=EPODOC&locale=de_EP&CC=WO&NR=2024223509A1&KC=A1&ND=4

Holmes J, Hafiz Y, Stachurski Z et al (2020) Surface topography evolution of woven thermoplastic composites under deformation. Compos B Eng. https://doi.org/10.1016/j.compositesb.2020.107880

MZ Islam, MA Rahman, L Gibbon, et al (2024) Comparing Poisson Ratio Measurement of 3D Printed Continuous Fiber Reinforced Composites: Digital Image Correlation (DIC) vs. Video-Extensometer. Proceedings of ASME 2024 19th International Manufacturing Science and Engineering Conference, MSEC 2024 1:. https://doi.org/10.1115/MSEC2024-124117

Janeliukstis R, Chen X (2021) Review of digital image correlation application to large-scale composite structure testing. Compos Struct. https://doi.org/10.1016/J.COMPSTRUCT.2021.114143

Karahan M, Karahan N (2013) Influence of weaving structure and hybridization on the tensile properties of woven carbon-epoxy composites. J Reinf Plast Compos 33:212–222. https://doi.org/10.1177/0731684413504019

Lomov SV, Gusakov AV, Huysmans G et al (2000) Textile geometry preprocessor for meso-mechanical models of woven composites. Compos Sci Technol 60:2083–2095. https://doi.org/10.1016/S0266-3538(00)00121-4

Lomov SV, Bogdanovich AE, Ivanov DS et al (2009) A comparative study of tensile properties of non-crimp 3D orthogonal weave and multi-layer plain weave E-glass composites. Part 1: materials, methods and principal results. Compos Part A Appl Sci Manuf 40:1134–1143. https://doi.org/10.1016/j.compositesa.2009.03.012

Mahfuz H, Adnan A, Rangari VK et al (2004) Carbon nanoparticles/whiskers reinforced composites and their tensile response. Compos Part A Appl Sci Manuf 35:519–527. https://doi.org/10.1016/J.COMPOSITESA.2004.02.002

Munro WA, Carnaby GA, Carr AJ, Moss PJ (1997) Some textile applications of finite-element analysis part I: finite elements for aligned fibre assemblies. J Text Inst 88:325–338. https://doi.org/10.1080/00405000.1997.11090887

Naufal MI, Wong KJ, Israr HA, et al (2024) Digital image correlation technique for failure and crack propagation of fibre-reinforced polymer composites – A review

Nazir M, Shaker K, Nawab Y, Hussain R (2019) Performance of novel auxetic woven fabrics produced using Helical Auxetic Yarn. Mater Res Express. https://doi.org/10.1088/2053-1591/ab1a7e

Nguyễn H, Fangueiro R, Ferreira F, Nguyễn Q (2023) Auxetic materials and structures for potential defense applications: an overview and recent developments. Text Res

J 93(23–24):5268–5306. https://doi.org/10.1177/0040517523119343
Osada T, Nakai A, Hamada H (2003) Initial fracture behavior of satin woven fabric composites. Compos Struct 61:333–339. https://doi.org/10.1016/S0263-8223(03)00058-8
Pan B, Qian K, Xie H, Asundi A (2009) Two-dimensional digital image correlation for in-plane displacement and strain measurement: A review. Meas Sci Technol. https://doi.org/10.1088/0957-0233/20/6/062001
Patel J, Peralta P (2017) Characterization of deformation localization mechanisms in polymer matrix composites: A digital image correlation study. Conference Proceedings of the Society for Experimental Mechanics Series 0:243–246. https://doi.org/10.1007/978-3-319-51439-0_58
Pickering KL, Efendy MGA, Le TM (2016) A review of recent developments in natural fibre composites and their mechanical performance. Compos Part A Appl Sci Manuf 83:98–112. https://doi.org/10.1016/J.COMPOSITESA.2015.08.038
Rajesh M, Singh SP, Pitchaimani J (2018) Mechanical behavior of woven natural fiber fabric composites: Effect of weaving architecture, intra-ply hybridization and stacking sequence of fabrics. J Ind Text 47:938–959. https://doi.org/10.1177/1528083716679157/ASSET/IMAGES/LARGE/10.1177_1528083716679157-EQ7.JPEG
Shan M, Zhao L, Ye J (2022) A novel micromechanics-model-based probabilistic analysis method for the elastic properties of unidirectional CFRP composites. Materials (Basel) 15:5090. https://doi.org/10.3390/MA15155090
Sun G, Tong S, Chen D et al (2018) Mechanical properties of hybrid composites reinforced by carbon and basalt fibers. Int J Mech Sci 148:636–651. https://doi.org/10.1016/J.IJMECSCI.2018.08.007
Ungerer B, Müller U, Pramreiter M et al (2022) Influence of yarn structure and coating on the mechanical performance of continuous viscose fiber/epoxy composites. Polym Compos 43:1012–1021. https://doi.org/10.1002/PC.26430
Venkateshwaran N, ElayaPerumal A, Arwin Raj RH (2012) Mechanical and dynamic mechanical analysis of woven banana/epoxy composite. J Polym Environ 20:565–572. https://doi.org/10.1007/S10924-011-0410-5
Wang Y, Sun W, Cao L (2024) Tensile and flexural mechanical attributes of hybrid carbon/basalt fiber metal laminates under various hybridization and stacking sequences. Compos Part A Appl Sci Manuf. https://doi.org/10.1016/j.compositesa.2023.107942
Wei G, Edwards SF (1998) Poisson ratio in composites of auxetics. Phys Rev E 58:6173–6181. https://doi.org/10.1103/PhysRevE.58.6173
Yan L, Chouw N, Jayaraman K (2014) Flax fibre and its composites – a review. Compos B Eng 56:296–317. https://doi.org/10.1016/J.COMPOSITESB.2013.08.014
Zhao C, Ren R, Zhong J et al (2022) Intralaminar crack propagation of glass fiber reinforced composite laminate. Structures 41:787–803. https://doi.org/10.1016/J.ISTRUC.2022.05.064
Zhou G, Sun Q, Meng Z et al (2021) Experimental investigation on the effects of fabric architectures on mechanical and damage behaviors of carbon/epoxy woven composites. Compos Struct. https://doi.org/10.1016/j.compstruct.2020.113366
Ziaja D, Jurek M, Śliwa R et al (2024) DIC application for damage detection in FRP composite specimens based on an example of a shearing test. Archives of Civil and Mechanical Engineering 24:1–13. https://doi.org/10.1007/S43452-024-00859-Z/METRICS

Publisher's Note Springer Nature remains neutral with regard to jurisdictional claims in published maps and institutional affiliations.